© 2017. Published by The Company of Biologists Ltd | Development (2017) 144, 3968-3977 doi:10.1242/dev.151381

Direct and efficient transfection of mouse neural stem cells and mature neurons by *in vivo* mRNA electroporation

Stéphane Bugeon[1], Antoine de Chevigny[1], Camille Boutin[1], Nathalie Coré[1], Stefan Wild[2], Andreas Bosio[2], Harold Cremer[1,*,‡] and Christophe Beclin[1,*]

ABSTRACT

In vivo brain electroporation of DNA expression vectors is a widely used method for lineage and gene function studies in the developing and postnatal brain. However, transfection efficiency of DNA is limited and adult brain tissue is refractory to electroporation. Here, we present a systematic study of mRNA as a vector for acute genetic manipulation in the developing and adult brain. We demonstrate that mRNA electroporation is far more efficient than DNA electroporation, and leads to faster and more homogeneous protein expression *in vivo*. Importantly, mRNA electroporation allows the manipulation of neural stem cells and postmitotic neurons in the adult brain using minimally invasive procedures. Finally, we show that this approach can be efficiently used for functional studies, as exemplified by transient overexpression of the neurogenic factor Myt1l and by stably inactivating Dicer nuclease *in vivo* in adult born olfactory bulb interneurons and in fully integrated cortical projection neurons.

KEY WORDS: Adult neurogenesis, Subventricular zone, Olfactory bulb, Cortex, Dicer, microRNA pathway

INTRODUCTION

Manipulation of gene expression in the brain of living animals represents a key approach in neurobiological research today. Over the past decades, mouse genetic approaches have been developed and widely used to study biological processes either via ectopic/overexpression or gene knockout in transgenic mice. However, the generation of genetically modified mice is a long-term project that requires considerable resources and infrastructure. Moreover, overexpression or inactivation of a given gene in a specific tissue/cell type or at a defined moment implicates complex strategies involving the concomitant presence of several transgenes in a given animal, rendering this approach expensive and time-consuming.

Several methods were developed to express transgenes in specific cell populations of living animals, including neurons. Viral vectors have been widely used for *in vivo* gene function studies or even therapeutic approaches (Kotterman and Schaffer, 2014; Papale et al., 2009). Although these tools allow the relatively rapid manipulation of defined brain structures, safety issues and immune reactions in the host tissue represent considerable limitations for their use (Lowenstein et al., 2007; Sack and Herzog, 2009).

Electroporation of plasmid DNA expression constructs to induce overexpression or knockdown of protein-coding genes or microRNAs (miRNAs) is nowadays a broadly used approach in studies of the developing and postnatal mouse brain (De Vry et al., 2010). However, DNA electroporation is of limited efficiency and allows generally only the targeting of embryonic (Saito and Nakatsuji, 2001) and early postnatal neural stem cell compartments (Boutin et al., 2008, 2010). Postmitotic neurons or adult neural stem cells in the subventricular compartment are highly refractory to DNA electroporation (Barnabé-Heider et al., 2008; De la Rossa and Jabaudon, 2014), even though some invasive techniques were developed to locally electroporate adult mature neurons (Molotkov et al., 2010; Ohmura et al., 2015; Pagès et al., 2015; Porrero et al., 2016).

In specific experimental models, such as *Ciona* or *Xenopus Laevis* oocytes, mRNA injection was extensively and efficiently used for ectopic gene expression or knockdown (Bertrand et al., 2003; Mimoto and Christian, 2011). Recently, mRNA transfection of combination of different transcription factors has been used *in vitro* in human cells to reprogram somatic cells into induced pluripotent stem cells (Luni et al., 2016) and to drive the neuronal differentiation of progenitor cells into specific neuronal cell types (Faedo et al., 2016). Based on these findings, we investigated the potential of *in vitro*-generated mRNAs for functional studies in the mouse brain. We show that mRNA electroporation is considerably more efficient than DNA for targeting the postnatal neural stem cell pool and leads to more homogeneous expression levels. mRNA-based protein expression is stable over days. Importantly, mRNA electroporation allows efficient targeting of neural stem cells in the adult ventricular/subventricular zone (VZ-SVZ) and even fully mature neurons integrated in the cortex and other brain structures. We demonstrate the usefulness of mRNA electroporation for functional analyses in the adult brain. First, we reveal that transient expression of the neuronal gene Myt1l can drive the transformation of neural stem cells into proliferative progenitors. Second, we show that stable recombination of the Dicer locus through CRE-mRNA electroporation in adult neural stem cells and layer 5 mature cortical neurons interferes with dendritic spine morphology and density, providing new *in vivo* evidence for the involvement of the microRNA pathway in synapse regulation.

RESULTS

Increased efficiency of postnatal electroporation using mRNAs

Postnatal *in vivo* brain electroporation allows the transfection of DNA constructs into the stem cell compartment surrounding the walls of the lateral ventricles (LV). Position of the electrodes around the head of the animal, and therefore the orientation of the electric field, allows specific targeting of the lateral or dorsal aspects of the ventricular wall (Boutin et al., 2008; de Chevigny et al., 2012; Fernández et al., 2011) (Fig. 1A). Electroporation of the lateral wall of the LV with an expression plasmid coding enhanced green fluorescent protein (EGFP) (pCAGGS-EGFP, 2 µl of a 5 µg/µl solution) produced at

[1]Aix-Marseille University, CNRS, IBDM UMR 7288, Marseille 13009, France.
[2]Miltenyi Biotec, Bergisch-Gladbach 51429, Germany.
*These authors contributed equally to this work

‡Author for correspondence (harold.cremer@univ-amu.fr)

H.C., 0000-0002-8673-5176

Received 1 March 2017; Accepted 21 September 2017

Development (2017) 144, 3968-3977 doi:10.1242/dev.151381

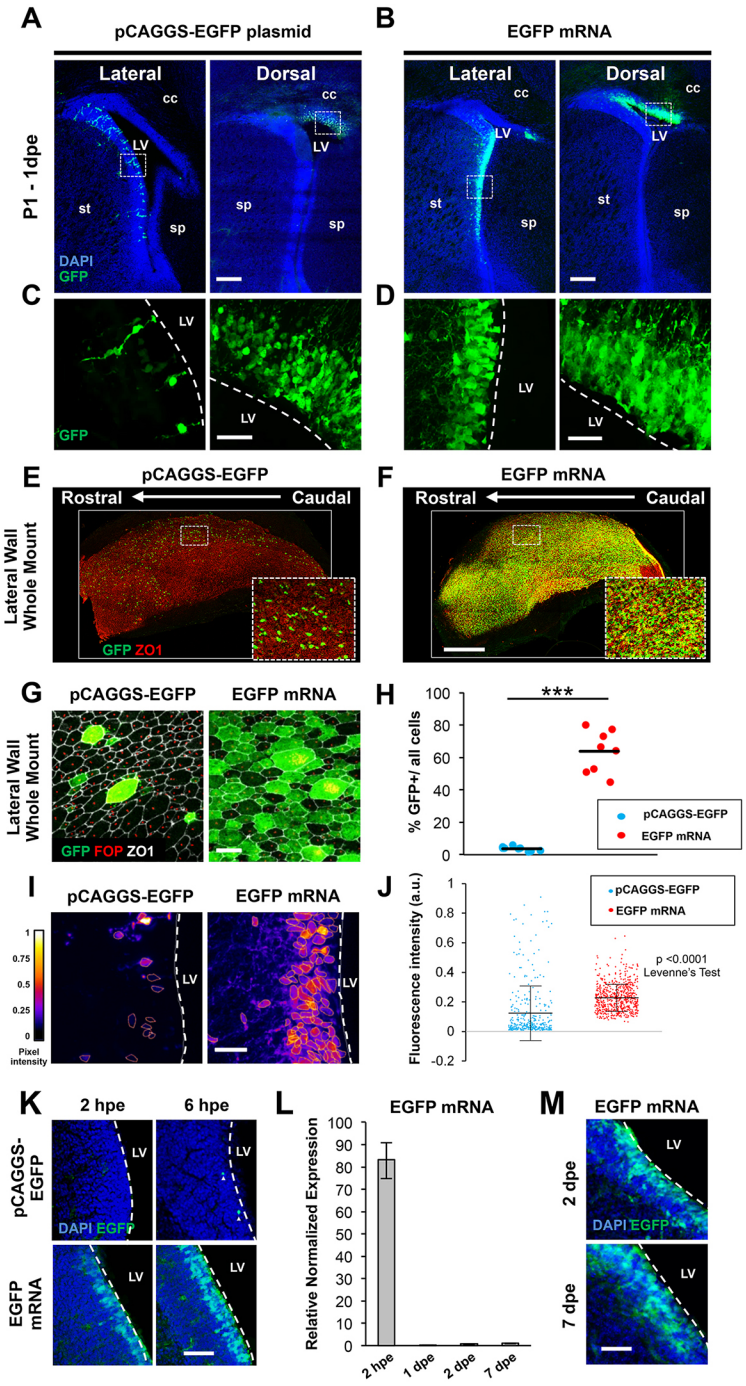

Fig. 1. EGFP mRNA electroporation efficiently labels the postnatal stem cell compartment. (A,B) Coronal sections of P1 pups electroporated with either a pCAGGS-EGFP plasmid or EGFP mRNAs, and sacrificed at 1 dpe. Dorsal and lateral walls of the lateral ventricle (LV) can be efficiently targeted via mRNA electroporation. Scale bars: 200 µm. LV, lateral ventricle; sp, septum; st, striatum; cc, corpus callosum. (C,D) Higher magnifications showing highly efficient transfection for mRNA electroporation. Dotted lines represent the border between VZ-SVZ and the LV. Scale bars: 30 µm. (E,F) Ventricular lateral wall wholemounts were prepared at 1 dpe after pCAGGS-EGFP or EGFP mRNA electroporation. Scale bars: 400 µm. (G) Higher magnifications of lateral wall wholemounts allowed precise quantification of the transfection efficiency for both conditions. Scale bar: 10 µm. In E-G, ZO1 labels tight junctions and FOP labels basal bodies. (H) Percentage of $EGFP^+$ cells among all the cells lining the lateral wall of the ventricle targeted by pCAGGS-EGFP versus EGFP mRNAs. *n*=3 animals, three areas/animal, horizontal bars indicate mean; *P*<0.0001, Wilcoxon rank sum test for means. (I) Color-coded EGFP intensity levels of electroporated cells lining the LV. Scale bar: 30 µm. (J) Quantification of mean cytoplasmic EGFP intensity. Individual points represent cells. Horizontal bars indicate mean, error bars indicate s.d. pCAGGS-EGFP, 0.12±0.01; EGFP mRNA, 0.23±0.004 a.u., *n*=337 and 616 cells, respectively, from three different animals; ***P<0.0001, Wilcoxon rank sum test for means; ***P<0.0001, Levene's test for homogeneity of variance. (K) P1 pups were electroporated with either a pCAGGS-EGFP plasmid or EGFP mRNAs, and sacrificed 2 h or 6 h after electroporation. EGFP fluorescence is detectable as early as 2 hpe using mRNA electroporation. Scale bar: 100 µm. (L) P1 CD1 mice were electroporated with EGFP mRNA and SVZ tissues were microdissected at 2 hpe, 1 dpe, 2 dpe and 7 dpe. RNA was then extracted and qRT-PCR carried out. We found very high EGFP mRNA expression at 2 hpe, which dramatically decreased at 1, 2 and 7 dpe: 2 hpe, 83.2±8.4; 1 dpe, 0.1±0.01; 2 dpe, 0.7±0.07; 7 dpe, 1±0.12; *n*=3 animals. Data are mean±s.e.m. (M) P1 pups were electroporated with EGFP mRNA and fluorescence was then compared at 2 and 7 dpe. EGFP fluorescence is still detectable at 7 dpe. Scale bar: 50 µm.

1 day post-electroporation (dpe) a typical sparse salt-and-pepper labeling with clearly distinguishable individual cells that showed radial glia morphology (Fig. 1A,C). DNA electroporation of the dorsal wall led generally to higher $EGFP^+$ cell densities. In both, lateral and dorsal compartments, EGFP intensity was highly variable between individual cells (Fig. 1C).

We followed the same experimental protocol using *in vitro*-synthesized mRNA encoding EGFP (StemMACS, EGFP mRNA, Miltenyi Biotec; 2 µl at 0.5 µg/µl, approximately equimolar to the used DNA concentration). As for DNA, orientation of the electroporation electrodes allowed the specific targeting of the lateral or dorsal VZ-SVZ domains (Fig. 1B). Both, lateral and dorsal electroporation of mRNA induced considerably stronger EGFP labeling of the ventricular walls at 1 dpe (Fig. 1D) compared with DNA-based transfection.

To quantitatively evaluate the targeting efficiency of neural stem cells by DNA versus mRNA electroporation, we analyzed ventricular Lateral Wall Whole Mount (LWWM) (Mirzadeh et al., 2008) preparations at 1 dpe. Low-magnification views of the lateral walls after DNA electroporation showed scattered EGFP staining with varying fluorescence levels among positive cells (Fig. 1E,G). In contrast, mRNA efficiently and homogeneously labeled the almost entire lateral wall of the lateral ventricle (Fig. 1F,G).

High-magnification images of whole-mount preparations (Fig. 1G) allowed us to precisely quantify the percentage of EGFP-positive cells in the ventricular wall. Overall, there was a

Development (2017) 144, 3968-3977 doi:10.1242/dev.151381

17-fold increase in the amount of transfected cells after mRNA electroporation compared with DNA (Fig. 1G,H).

We then quantified the mean EGFP fluorescence intensity in individual electroporated cells on LV coronal sections. The vast majority of DNA electroporated cells were poorly fluorescent. Only a small fraction showed very high intensity levels. In contrast, after mRNA electroporation almost all cells were intensely fluorescent (Fig. 1J). Moreover, the mean EGFP fluorescence intensity among individual electroporated cells (Fig. 1I,J) showed a twofold lower standard deviation after mRNA electroporation compared with DNA (Fig. 1J). Thus, mRNA electroporation, in addition to targeting more cells, led to more homogenous protein levels in electroporated neural stem cells than using DNA plasmids (Fig. 1I,J). Moreover, EGFP fluorescence level per cell varies with the mRNA concentration, permitting control of protein concentration in gain-of-function situations (Fig. S1). The impact of transcript size on electroporation efficiency and protein expression has not been studied in the context of this work. In conclusion, *in vivo* mRNA electroporation provides an efficient means of labeling postnatal neural stem cells, improving both the rate and homogeneity of electroporation compared with the use of plasmid DNA.

Time-course of expression of electroporated mRNA

We investigated the dynamics of protein appearance after mRNA versus DNA electroporation. Two hours after lateral DNA electroporation, fluorescence was undetectable. After 6 h sparsely distributed individual cells were EGFP positive (Fig. 1K). In contrast, mRNA electroporation induced homogeneous EGFP fluorescence in large amounts of cells as early as 2 h after electroporation, which increased in intensity at 6 h (Fig. 1K). Thus, in agreement with the absence of need for a transcription step, protein production was considerably faster after mRNA electroporation compared with DNA.

Next we investigated the stability of mRNA over time after *in vivo* electroporation. mRNA electroporation followed by microdissection of VZ-SVZ tissue and qRT-PCR (quantitative reverse transcription polymerase chain reaction) for the presence of EGFP mRNA demonstrated that, at 2 h post electroporation, high quantities of transcript could be detected. However, at 1, 2 and 7 dpe very low EGFP mRNA levels were present, indicating rapid degradation of transcripts (Fig. 1L). Nevertheless, EGFP fluorescence was detectable until 7 dpe, pointing towards the high stability of EGFP protein in cells (Fig. 1M) (Corish and Tyler-Smith, 1999). Thus, although electroporated mRNAs generate high quantities of protein during a short period, active protein can be identified for prolonged periods.

Highly efficient transgene expression via CRE mRNA electroporation

The above results show that mRNA electroporation allows the highly efficient transient expression of exogenous proteins *in vivo*. In the next steps, we aimed to combine the efficiency of mRNA electroporation with the permanent genetic modifications induced by CRE-loxP-induced recombination to allow long-term cell-tracing and gene-function analysis.

First, we asked whether CRE/loxP mRNA-mediated recombination could be used for the efficient long-term labeling of defined stem cell and neuron populations *in vivo*. During postnatal neurogenesis, the vast majority of newborn olfactory bulb (OB) neurons is generated from the lateral ventricle walls and populates mainly deep positions of the OB after migration. Smaller subsets are generated from the dorsal and medial aspects, and integrate mainly into the superficial layers of the granule cell layer (GCL) and the glomerular layer (GL) (Merkle et al., 2007).

We electroporated mRNA encoding CRE recombinase (StemMACS CRE Recombinase mRNA, Miltenyi Biotec; 0.5 µg/µl) into the lateral and medial aspects of the forebrain ventricles of newborn R26-*Ai14* mouse pups, carrying a CRE-inducible tomato allele in the ROSA26 locus (Madisen et al., 2010). Twenty-one days later large parts of the lateral and medial ventricular walls showed strong tomato fluorescence, demonstrating efficient recombination in the stem cell compartment (Fig. 2A). Consistent with this high transfection level, we observed large amounts of cells in the rostral migratory stream (Fig. 2C) as well as many postnatally generated tomato-positive neurons in the OB (Fig. 2D-F). After lateral electroporation, these fluorescent neurons were predominantly localized in deep positions in the GCL (Fig. 2D,E) whereas after medial electroporation they settled mainly in the GL (Fig. 2D,F), in agreement with the localization of the respectively targeted stem cell pools (Fernández et al., 2011). Moreover lateral electroporation labeled numerous fluorescent astrocytes in the striatum (Fig. 2B). Together, these results show that combining the efficiency of mRNA electroporation with the permanence of CRE recombination is a powerful approach with which to label and manipulate large amounts of newborn cells in the postnatal mouse brain. We also

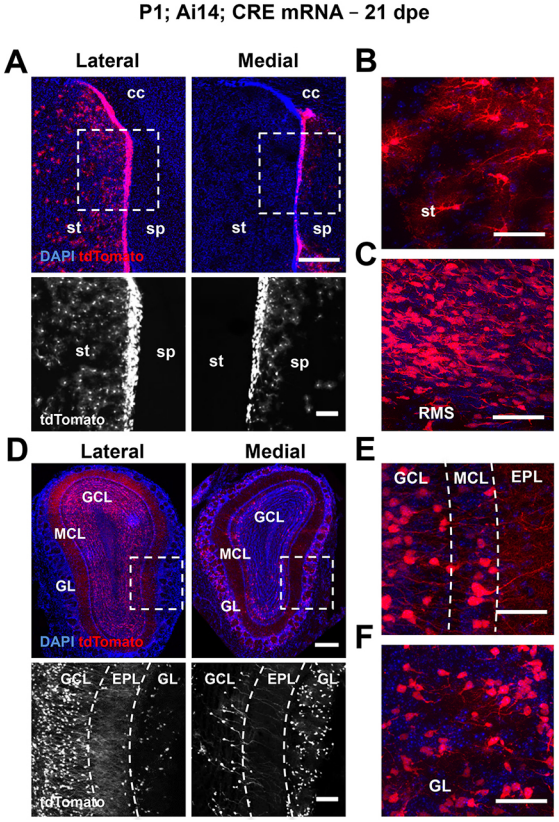

Fig. 2. *In vivo* CRE mRNA electroporation allows highly efficient and stable genetic recombination. (A) Coronal sections representing the VZ-SVZ of Ai14 mice electroporated either laterally or medially at P1 with CRE mRNA 21 days after electroporation. Scale bars: 300 µm; 100 µm for higher magnifications. sp, septum; st, striatum; cc, corpus callosum. (B,C) High magnifications of VZ-SVZ-originating astrocytes populating the striatum (B) and neuroblasts in the rostral migratory stream (RMS) (C). Scale bars: 50 µm. (D) Cellular distribution at 21 dpe in the olfactory bulb after lateral or medial electroporation of CRE mRNA in P1 Ai14 mice. Scale bars: 300 µm; 100 µm for higher magnifications. GCL, granule cell layer; MCL, mitral cell layer; EPL, external plexiform layer; GL, glomerular layer. (E,F) High magnifications of recombined granule cells (E) and periglomerular neurons (F) on olfactory bulb coronal sections. Scale bars: 50 µm.

Development (2017) 144, 3968-3977 doi:10.1242/dev.151381

found that CRE mRNA is suited to efficiently induce recombination in the embryonic forebrain (Fig. S2).

CRE mRNA-mediated recombination of adult neural stem cells

Although DNA electroporation is routinely used to study embryonic and postnatal neurogenesis, adult neurogenesis of the olfactory bulb is only poorly targeted by this approach. Here, current *in vivo* transfection strategies rely on the use of virus infection, which does not allow the targeting of defined subregions of the ventricular walls. We asked whether mRNA electroporation could be used to overcome these limitations.

Electroporation of a pCAGGS-CRE plasmid (10 µg/µl) in the lateral wall of 8-week-old *R26-Ai14* mice resulted in the appearance of individualized cells in the ventricular wall at 5 dpe. These cells had generally the typical cuboid morphology of ependymocytes (Fig. 3A). When CRE mRNA (0.5 µg/µl) was used under the same conditions, 5 days later the entire lateral wall was covered with tdTomato-positive cells (Fig. 3A). High magnification images and S100β immunostaining validated ependymal targeting (Fig. 3A,B, yellow arrowheads). Moreover, individual cells in subependymal positions and extending basal processes showed tdTomato fluorescence (Fig. 3B, white arrowheads). Position, morphology and the observation that many of these cells expressed the glial marker GFAP (glial fibrillary acidic protein) indicated that they were adult B1-type neural stem cells (Fig. 3A,B). Supporting this observation, ventricular lateral wall whole-mount preparations of CRE mRNA-electroporated animals at 5 dpe showed characteristic pinwheel structures (Mirzadeh et al., 2008) with recombined multi-ciliated ependymocytes (white dotted line) surrounding recombined mono-ciliated B1 stem cells (white arrowhead in Fig. 3C).

In accordance with the previous observation that adult neural-stem cells could be targeted by mRNA electroporation, 28 days after CRE mRNA electroporation animals displayed a substantial amount of adult-born neurons in the olfactory bulb (Fig. 3D,E). This was strikingly different from DNA electroporations in which OB neurons were observed only sporadically (Fig. 3D-F). Thus, mRNA electroporation allowed the efficient and reliable genetic manipulation of adult neural stem cells and their derivatives.

Next, we asked whether it was possible to target mRNA to specific adult VZ-SVZ subregions, and subsequently label neurons integrated in specific layers of the OB (Fig. 4A), comparable with the situation in postnatal animals. Both the dorsal and lateral walls could be labeled by CRE mRNA electroporation into Ai14 mice. Both targeted compartments gave rise to new olfactory interneurons at 28 dpe, with lower amounts of cells generated from dorsal electroporations (Fig. 4B), as expected. We analyzed the distribution of the adult generated cells in the OB. Similar to what we observed with postnatal electroporation, lateral electroporation strongly biased the neuronal production towards deep granule cells, whereas dorsal electroporation mostly generated superficial granule cells and periglomerular cells (Fig. 4C). Thus, mRNA electroporation represents an efficient new tool with which to manipulate forebrain neurogenesis and neural stem cell regionalization in the adult mouse brain.

Mature neurons in adult animals can be efficiently electroporated with mRNA

Postmitotic neurons in the adult brain are refractory to transfection with DNA (De la Rossa and Jabaudon, 2014). We investigated whether the use of mRNA could overcome this limitation. Intra-parenchymal injection of CRE mRNA in adult R26-Ai14 mice was followed by electroporation (Fig. 5A). This approach reliably targeted

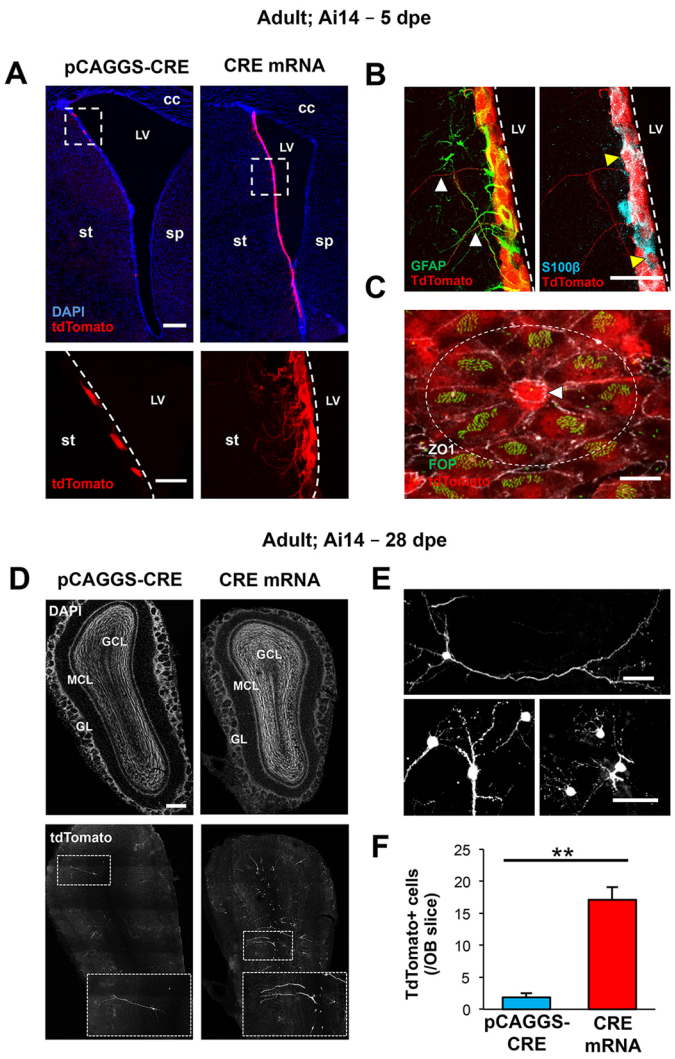

Fig. 3. mRNA electroporation efficiently targets adult neural stem cells. (A) Adult mice were electroporated with either a pCAGGS-CRE plasmid or CRE mRNA. Coronal sections of the rostral VZ-SVZ show higher recombination for CRE mRNAs. Scale bars: 200 µm; 30 µm for higher magnifications (lower panels). (B) High magnification of an adult VZ-SVZ electroporated with CRE mRNA showing characteristic B1 apical cells labeled with GFAP (white arrowheads) and ependymocytes labeled with S100B (yellow arrowheads). Scale bar: 30 µm. (C) Ventricular LWWM of CRE mRNA-electroporated adult mice at 5 dpe. Most labeled cells show the typical morphology of ependymocytes. B1 apical cells (white arrowhead) were also targeted by mRNA electroporation, as shown by the pinwheel structure indicated by a white dotted line. ZO1 labels tight junctions and FOP basal bodies. Scale bar: 10 µm. (D) Olfactory bulb coronal sections were taken 28 days after electroporation of pCAGGS-CRE or CRE mRNA in adult mice. Scale bar: 200 µm. (E) Representative higher magnifications of granule cells and periglomerular neurons recombined by CRE mRNA adult electroporation. Scale bars: 100 µm. (F) Quantification of the mean number of labeled neurons per OB slice 28 days after pCAGGS-CRE or mRNA CRE electroporation shows eight times higher efficiency with CRE mRNA electroporation. pCAGGS-CRE, 1.9±0.7; CRE mRNA, 17.1±2.0, n=5-6 animals; $^{**}P$=0.0043, Wilcoxon rank sum test. Data are mean±s.e.m.

mature neurons in different regions of adult brain, including layer 5 pyramidal neurons in S1 somatosensory cortex (Fig. 5B), medium spiny neurons of dorsal striatum (Fig. 5E) and medial septum neurons (Fig. 5G), allowing the study of neuronal morphology at synaptic resolution (Fig. 5C,F,H). Injected but non-electroporated control brains never showed tdTomato-positive cells.

Development (2017) 144, 3968-3977 doi:10.1242/dev.151381

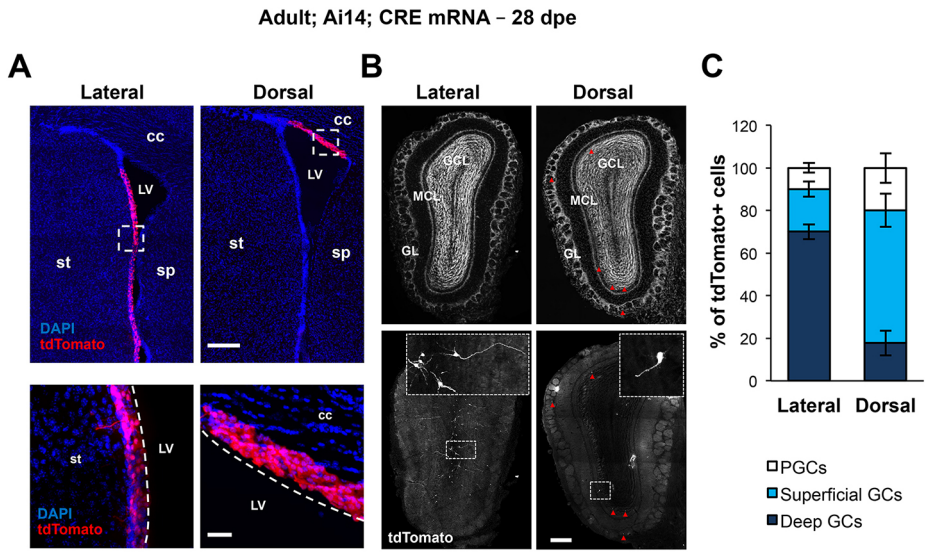

Fig. 4. mRNA electroporation allows analysis of the contribution of different lateral ventricular walls during adult neurogenesis. (A) Photomicrograph of the lateral ventricle 28 days after lateral versus dorsal electroporation of CRE mRNA in adult mice. Scale bars: 200 µm (top); 30 µm (bottom). (B) Olfactory bulb coronal sections taken 28 days after CRE mRNA electroporation to adult Ai14 mice showing successfully recombined neurons (red arrowheads). Dorsal electroporation generated fewer recombined neurons than lateral electroporation. Scale bar: 200 µm. (C) Quantification of the different neuronal cell types generated after electroporation of lateral versus dorsal adult neural stem cells among the total number of tdTomato-positive cells in the olfactory bulb. The proportion of superficial GCs generated by adult dorsal electroporation is much higher than after adult lateral electroporation. Lateral electroporation: 70.1±3.5, 20.1±3.5 and 9.9±2.3% of cells; dorsal electroporation: 17.8±5.8, 62.3±7.7 and 19.9±7.0% of cells (for deep GC, superficial GC and PGC, respectively). Data are mean±s.e.m.

Electroporated cells were mostly located close to the injection site, likely reflecting low diffusion of mRNA in the tissue. In addition to mature neurons, about 20% of the targeted cells were NeuN negative. These cells showed typical astrocytic morphologies and over 90% expressed the glial marker GFAP, altogether showing that mRNA electroporation targets preferentially, but not exclusively, neurons (Fig. 5D). Overall, our results show that CRE mRNA electroporation efficiently transfects adult postmitotic and fully integrated neurons in different brain areas.

Functional analyses based on mRNA electroporation

Next, we provided proof of principle that mRNA electroporation can be used for functional analyses using both gain- and loss-of-function approaches. As a prerequisite, we investigated the degree of co-transfection when two mRNAs were used in parallel. Co-electroporation of equal amounts of EGFP and CRE mRNA at P1 showed that almost 70% of all fluorescent cells were double positive at 1 dpe (Fig. 6A,B). Thus co-expression of two proteins by mRNA electroporation is efficient.

On the basis of this, we first performed a gain-of-function approach. The pan-neuronal basic helix-loop-helix transcription factor Myt1l has been implicated in the acquisition of neuronal identity by repressing non-neuronal fates (Mall et al., 2017). Moreover, expression of Myt1l, together with Brn2 and Ascl1, has been used for the induction of highly proliferative neuronal precursors from fibroblasts (Lim et al., 2015).

We investigated the consequences of Myt1l overexpression in postnatal neural stem cells. Co-electroporation of equal amounts of EGFP and Myt1l mRNAs at P1 led to increased numbers of BrdU-positive cells in the SVZ at 2 dpe (Fig. 6C,D), in agreement with the induction of additional proliferative interneuron precursors.

In the next step we performed a loss-of-function approach, thereby focusing on the microRNA pathway. Dicer is a cytoplasmic nuclease that is essential for the biogenesis of functional microRNAs. Dicer mutant mice have been widely used to study the microRNA pathway *in vivo*. However, constitutive or conditional loss of function for Dicer in mice induces severe developmental phenotypes, rendering the analyses of late and/or cell-autonomous roles of the microRNA pathway difficult (Bernstein et al., 2003). Nevertheless, specific microRNAs have been implicated in the control of synapse formation and plasticity in the developing and adult brain (Pathania et al., 2012; Siegel et al., 2011).

Based on these observations, we asked whether CRE-mRNA electroporation could be used to study the consequences of Dicer deficiency on synaptic spine density and structure in adult-generated OB neurons and fully mature cortical projection neurons. We generated a double transgenic mouse line harboring a conditional Dicer allele ($Dicer^{flox}$) (Harfe et al., 2005) and the Ai14 allele (see above) to allow detection of recombination events and morphological analysis at synaptic resolution. First, we investigated Dicer function during adult OB neurogenesis. We performed intraventricular injection of CRE-mRNA in 2-month-old $Dicer^{wt/flox}$ and $Dicer^{flox/flox}$ mice, and electroporated into adult neural stem cells of the lateral wall. Analyses of adult-born granule cells at 28 dpe (Fig. 6E) revealed a 30% decrease in the density of apical tuft dendritic spines (Fig. 6F), without any significant difference regarding the length of these spines (Fig. 6G).

Next, we asked whether Dicer expression is essential for the maintenance of a correct spine density and structure in integrated and fully mature cortical neurons that were generated during embryogenesis. We performed intra-parenchymal injection of CRE-mRNA into the adult neocortex of $Dicer^{wt/flox}$ and $Dicer^{flox/flox}$ mice and investigated spine density and morphology of recombined layer 5 pyramidal neurons of S1 somatosensory cortex (Fig. 6H). Quantitative analyses at 28 dpe revealed no change in spine density (Fig. 6I). However, in this situation dendritic spine length was significantly decreased (Fig. 6J).

Thus, we show that mRNA electroporation is an efficient and alternative method to analyze gene function in the brain. We show

Development (2017) 144, 3968-3977 doi:10.1242/dev.151381

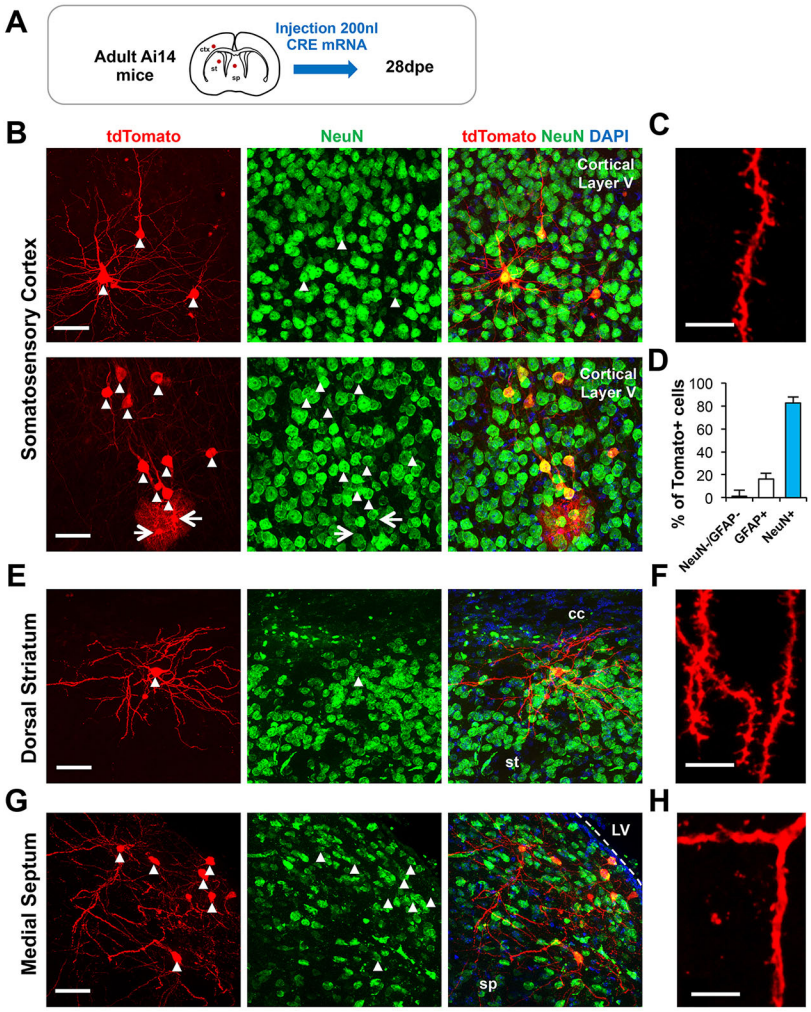

Fig. 5. Mature neurons in the parenchyma of adult mice can be electroporated by mRNAs. (A) Adult Ai14 mice were injected with CRE mRNAs in three different brain regions: somatosensory cortex, striatum or septum. The intra-parenchymal injection was followed by electroporation and the brains were taken for analysis at 28 dpe. Mature neurons were efficiently targeted in all three regions. (B-D) Somatosensory cortex electroporations. (B) Photomicrograph showing three cells in layer 5, with the typical morphology of glutamatergic excitatory neurons. Lower panels: another picture in layer 5 somatosensory cortex with neurons (white arrowheads) and astrocytes (white arrows). (C) High magnification of a representative dendrite showing synaptic resolution. (D) Quantification of the contribution of $NeuN^+$ and $GFAP^+$ cells in somatosensory cortex electroporations. Eighty percent of the labeled cells are neurons. In the non-neuronal fraction, most of the cells expressed GFAP. Data are mean±s.e.m. (E,F) Striatal electroporation efficiently targets medium spiny neurons (white arrowheads) (E) with synaptic resolution (F). (G,H) Septal electroporation. The majority of targeted cells are $NeuN^+$ cells (white arrowheads) (G) that have few dendritic spines, as expected (H). Scale bars: 50 µm for B,E,G; 5 µm for C,F,H.

that overexpression of a transcription factor by this approach interferes with proliferation in postnatal neural stem cells. When applied to Dicer-conditional mutant mice, we demonstrate a function of the microRNA pathway in synaptic spine density and architecture in the adult brain.

DISCUSSION

We show here that mRNA electroporation holds considerable advantages over classical approaches based on DNA electroporation. First, transfection efficiency *in vivo* using mRNA is greatly increased over DNA. Electroporation of equimolar amounts of mRNA and DNA led to an over 17-fold increase in the amount of EGFP-expressing cells along the ventricular wall of the forebrain. Transfection efficiency in electroporation is a function of the size of the used nucleic acid molecules (Ribeiro et al., 2012). Given that the EGFP mRNA is about ten times smaller than the corresponding DNA plasmid, its transfer into the cell might be facilitated. Moreover, certain cell types in the ventricular wall might be refractory to DNA-based expression but permissive for RNA. For example, in our hands postmitotic ependymocytes are difficult to electroporate with DNA constructs, while both EGFP and CRE mRNAs are efficiently expressed in this cell type. It is possible that the breakdown of the nuclear membrane during mitosis allows the introduction of episomal DNA into the nucleus, a key prerequisite for the generation of functional mRNA and subsequently protein. Once the nuclear membrane is stable and permanent, nuclear traffic becomes highly regulated and DNA transfer into the nucleus is not efficient anymore. In contrast, RNA does not need to enter the nucleus of target cells to be expressed.

It would have been interesting to investigate whether electroporation efficiency is similar between mRNA of significantly different sizes. However, analyzing the influence of mRNA size on electroporation efficiency has several drawbacks. For example, addressing this point based on the expression of a protein translated from the electroporated mRNA is biased by the detection threshold of each protein. On the other hand, direct measurement of the abundance of electroporated transcripts in electroporated cells is hampered by the short half-life of mRNAs in the cell and the potential impact of the diverging sequences on transcript stability.

Second, mRNA electroporation leads to faster and more homogeneous expression of transgenes. Once introduced into a cell, DNA needs to enter the nucleus in order to be transcribed into mRNA, which then needs to be re-exported to the cytoplasm for translation. In contrast, mRNA can be directly used for translation in the cytoplasm, leading to the very rapid accumulation of a wanted protein. Only 2 h after mRNA electroporation, EGFP fluorescence was detectable in the targeted cells. This rapid and homogeneous expression might be of major impact for functional studies. For example, major transcriptional regulators that control neural stem cell identity and fate might act during short and early time windows. mRNAs appear well suited to provide better quantitative and

Development (2017) 144, 3968-3977 doi:10.1242/dev.151381

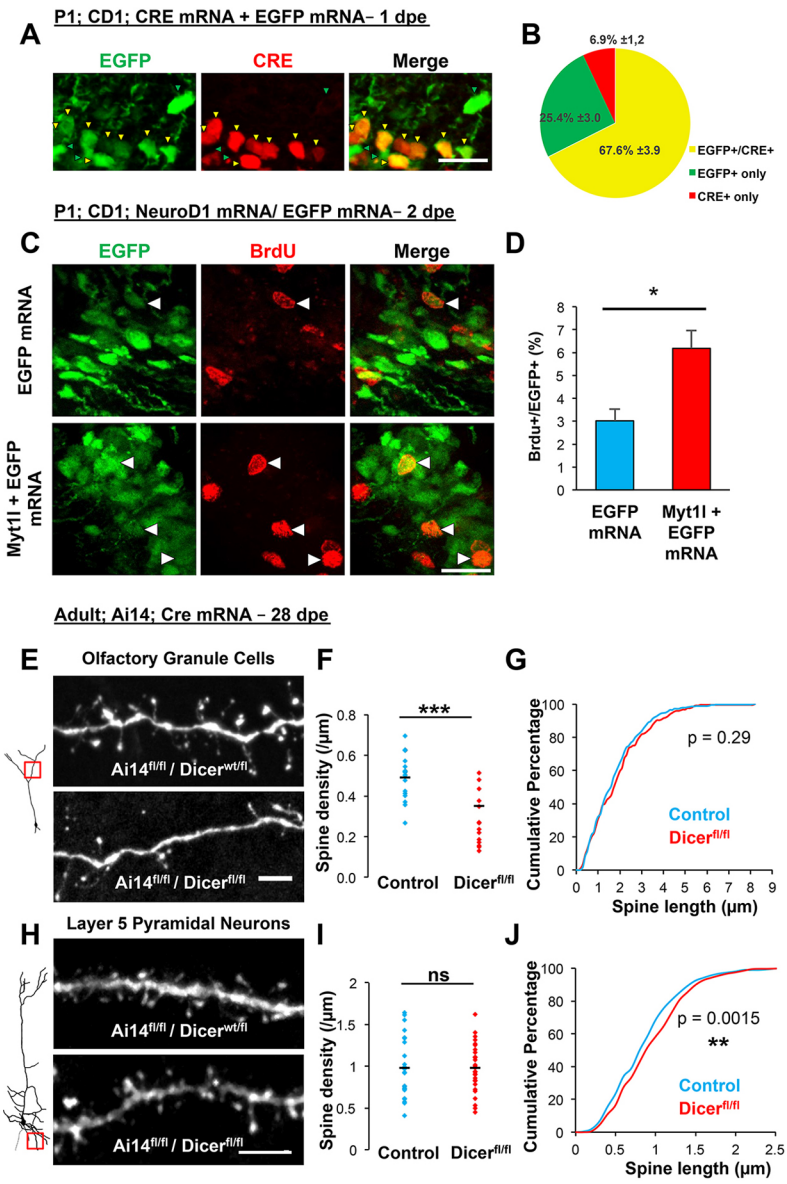

Fig. 6. Gene function analyses using mRNA electroporation. (A,B) P1 CD1 mice were electroporated with a mixture of CRE and EGFP mRNAs, at the same molarity (0.5 µg/µl each). (A) One day after electroporation, mice were sacrificed and fixed. Subsequently anti-CRE and anti-EGFP immunostainings were performed. Yellow arrowheads correspond to double-positive cells and green arrowheads to EGFP-positive cells. Scale bar: 20 µm. (B) Quantification of double- and single-labeled cells. (C) P1 CD1 mice were medially electroporated with either EGFP mRNA or EGFP+Myt1 l mRNA. Two days after electroporation, these animals were injected intra-peritoneally with a single dose of BrdU (at 50 mg/kg body weight). Two hours after injection, animals were sacrificed and BrdU-positive cells were revealed by anti-BrdU immunostaining. Arrowheads indicate $BrdU^+/EGFP^+$ cells. Scale bar: 20 µm. (D) The percentage of $BrdU^+$ cells among $EGFP^+$ cells in the medial SVZ was assessed and compared for both conditions. BrdU integration was increased after Myt1l gain of function. $BrdU^+/EGFP^+$ cells among $EGFP^+$ cells: EGFP mRNA, 3.02±0.52%; Myt1l+EGFP mRNA, 6.18±0.78%; *n*=6 animals and >1500 cells; *P*=0.0046, Wilcoxon rank sum test for means. Data are mean±s.e.m. (E-G) Dicer deletion in adult-generated olfactory neurons. Adult $Dicer^{wt/fl}$ and $Dicer^{fl/fl}$ mice were injected intraventricularly with CRE mRNAs and lateral electroporation was performed. (E) Olfactory bulb coronal sections were collected at 28 dpe, and high-resolution images of adult-born granule cells dendrites were taken in the EPL and analyzed. (F) Quantification of the mean spine density was obtained and compared for both genotypes, showing a large decrease in Dicer conditional mutant mice. $Dicer^{wt/flox}$, 0.49±0.027; $Dicer^{flox/flox}$, 0.35±0.038 spine/µm, *n*=33 and 21 cells from two animals for $Dicer^{wt/flox}$ and $Dicer^{flox/flox}$, respectively; ***$P<0.0001$, Wilcoxon rank sum test for means. Data are mean±s.e.m. (G) Spine length was not significantly altered by Dicer deletion in this conditions. $Dicer^{wt/flox}$, 1.77±0.059; $Dicer^{flox/flox}$, 1.9±0.085 µm, *n*=434 and 248 spines from 11 cells for $Dicer^{wt/flox}$ and $Dicer^{flox/flox}$, respectively; *P*=0.30, two-sample Kolgomorov–Smirnov test. Data are mean±s.e.m. (H-J) Dicer deletion in mature excitatory neurons of the adult somatosensory cortex. Adult layer V cortical pyramidal neurons were electroporated with CRE mRNA in $Dicer^{wt/fl}$ and $Dicer^{fl/fl}$ mice. (H) Basal dendrites were visualized at 28 dpe. (I) Quantification of the mean spine density revealed no significant difference between conditions. $Dicer^{wt/flox}$, 0.983±0.071; $Dicer^{flox/flox}$, 0.977±0.029 spine/µm, *n*=25 and 31 from four animals for $Dicer^{wt/flox}$ and $Dicer^{flox/flox}$, respectively; ns: non significant, Wilcoxon rank sum test for means. (J) In contrast, spine length was significantly increased by Dicer deletion. $Dicer^{wt/flox}$, 0.86±0.021; $Dicer^{flox/flox}$, 0.92±0.019 µm; *n*=465 and 522 spines from 10 cells for $Dicer^{wt/flox}$ and $Dicer^{flox/flox}$, respectively; **$P=0.0015$, two-sample Kolgomorov–Smirnov test. Scale bars: 5 µm in E,H.

temporal control. To exemplify this point, we were able to significantly induce the generation of proliferative progenitors by electroporating Myt1l mRNA into neural stem cells.

Third, mRNA electroporation can be used to conveniently manipulate both stem cells and postmitotic neurons in the adult brain. Currently, acute transgenesis in adult animals is mainly

Development (2017) 144, 3968-3977 doi:10.1242/dev.151381

performed by infection with recombinant viruses. However, this approach has some important limitations. For example the production and use of active viral particles demand particular safety measures, permissions and know-how, which are not always available. Moreover, virus infection can induce immunological reactions of the host tissue that can interfere with the analysis of a given phenotype (Lowenstein et al., 2007; Sack and Herzog, 2009).

The use of mRNA electroporation is limited by the shorter persistence of the electroporated RNA compared with DNA. To overcome this limitation, we combined RNA electroporation with CRE-LoxP-induced genetic manipulation to induce long-term changes in gene expression. Using this approach, we were able to efficiently and durably change gene expression in adult neurons of the olfactory bulb, after targeting adult neural stem cells of the VZ/SVZ region. Importantly, we were also able to alter gene expression in post-mitotic cortical projection neurons by simple intra-parenchymal injections of very small liquid volumes, thus avoiding severe disruption of the surrounding brain tissue. Previous approaches that demonstrated electroporation of DNA into neurons were of low efficiency and highly invasive, requiring the implantation of electrodes into the brain tissue (Molotkov et al., 2010; Ohmura et al., 2015; Pagès et al., 2015; Porrero et al., 2016). We provide the first non-viral method for transfecting adult neurons in different brain regions based on non-invasive surface electrodes.

Finally, we validated the mRNA electroporation approach to study gene function *in vivo* by investigating the role of the microRNA pathway in synapse formation and stability in adult brain. Modified expression of specific microRNAs was shown to impact dendritogenesis and spine formation in developing neurons (Bicker et al., 2014). Moreover, microRNAs were implicated in activity-dependent translation at the synapse (Cohen et al., 2011; Gu et al., 2015; Weiss et al., 2015). Alterations in such processes may lead to psychiatric disorders. For example, deregulation of miR-137 is associated with schizophrenia and mental disability in humans (Siegert et al., 2015).

So far, studies aiming at deciphering the role of microRNAs in synaptic functions have been performed *in vitro* and/or in a context where the change in microRNA expression was constitutive. The mRNA electroporation approach we present here reveals the specific involvement of the microRNA pathway in adult animals in the establishment of synapses during neurogenesis, as well as the maintenance of spine morphology in neurons that were already functionally integrated.

MATERIALS AND METHODS

Animals

CD1 (Charles-River, Lyon, France), Ai14 transgenic reporter (Jackson Laboratories, stock number 007914) and Dicer-floxed (Jackson Laboratories, stock number 006001) male and female mice were used. Animal experiments were carried out in accordance with European Communities Council Directive and approved by French ethical committees (Comité d'Ethique pour l'expérimentation animale no. 14; permission number: 62-12112012).

Plasmids and mRNA preparation

The pCAGGS-CRE and pCAGGS-EGFP vectors were derived from pCX-MCS2 (Morin et al., 2007). Both plasmids were used at a concentration of 5 µg/µl (0.1% Fast Green), except for adult electroporation (Fig. 3), where pCAGGS-CRE was used at 10 µg/µl.

mRNAs were provided by Miltenyi Biotec (Miltenyi Biotec): EGFP mRNA (130-101-114), CRE Recombinase mRNA (130-101-113) and Myt1l mRNA (130-104-379) (a kind gift from A. Bosio, Miltenyi Biotec). mRNAs were synthesized in an animal component-free production process using T7-based transcription from a cDNA vector (optimized with regard to human codon usage) and subsequent 5′ capping and 3′ polyadenylation. Optionally, Ψ-UTP- and 5-mCTP-modified nucleotides were introduced to reduce innate immune responses against mRNA in downstream applications. mRNAs were DNase treated, sterile filtered and lyophilized. mRNAs were then diluted in RNAse-free PBS at a concentration of 0.5 µg/µl (same range of molarity compared with 5 µg/µl DNA plasmid), except for Fig. S1, where mRNA concentrations are indicated.

Postnatal electroporation

Postnatal electroporation was performed as described previously (Boutin et al., 2008). Briefly, P1 pups were anesthetized by hypothermia. A glass micropipette was inserted into the lateral ventricle and 2 µl of plasmid or RNA solution was injected by expiratory pressure using an aspirator tube assembly (Drummond). Successfully injected animals were subjected to five 95 V electrical pulses (50 ms, separated by 950 ms intervals) using the CUY21 edit device (Nepagene) and 10 mm tweezer electrodes (CUY650P10, Nepagene) coated with conductive gel (Control Graphique Medical). Electroporated animals were reanimated in a 37°C incubator before returning to the mother.

In utero electroporation

Timed pregnant E15.5 CD1 mice were anesthetized and the uterine horns were exposed. CRE mRNA (at 0.5 µg/µl) was then injected into the lateral ventricle of the embryos with a glass micropipette by expiratory pressure using an aspirator tube assembly (Drummond). Fast Green was added at 0.01% for visualization of injection. Successfully injected animals were subjected to five 35 V electrical pulses (50 ms, separated by 950 ms intervals) using the CUY21 edit device (Nepagene) and 3 mm tweezer electrodes (CUY650P3, Nepagene).

Adult electroporation

Eight- to ten-week-old animals were deeply anesthetized intraperitoneally [3.0 mg of ketamine (Imalgene); 0.25 mg of xylazine (Rompun; Bayer)] and stereotaxically injected with 2 µl (injection in the lateral ventricle) or 200 nl (intraparenchymal injections) of nucleic acid solution using a Nanoject II (Drummond) equipped with a glass micropipette, at a rate of 230 or 23 nl/s, respectively. The coordinates for injections in the lateral ventricle were AP 0.0; L 1.0; V −1.5 mm, AP 0.2; L 2.0; V −0.8 mm for somato-sensory cortex; AP 0.2; L 0.5; V −2 mm for septum; and AP 0.2; L 2.0; V −2.5 mm for dorsal striatum, relative to Bregma. After injection, animals were subjected to five 200 V electrical pulses.

Lateral-wall whole mounts

Immunostaining of ventricular lateral-wall whole-mount (LWWM) preparations were carried out as described previously (Boutin et al., 2014). Briefly, dissected brains were subjected to a 12 min fixation in 4% paraformaldehyde+0.1% Triton X-100, blocked 1 h in PBS+3% BSA, incubated overnight with primary antibodies diluted in PBS, 0.1% Triton X-100 and 3% BSA, and incubated for 1 h with adapted secondary antibodies at room temperature. LWs were dissected further and mounted with Mowiol before imaging using confocal microscope (Leica SP8). Primary antibodies were rabbit anti-ZO1 (1:400; Thermo Fisher Scientific, 61-7300), mouse IgG1 anti-NeuN (1:100; Millipore, Mab 377) and chicken anti-EGFP (1:1000; Aves Labs, GFP-1010). Secondary antibodies were Alexa Fluor 647 goat anti-rabbit (1:800; Thermo Fisher Scientific, A-21244), Alexa Fluor 568 goat anti-mouse IgG2b (1:800; Thermo Fisher Scientific, A-21144), Alexa Fluor 488 goat anti-mouse IgG2b (1:800; Thermo Fisher Scientific, A-21141) and Alexa Fluor 488 donkey anti-chicken (1:500; Jackson ImmunoResearch, 703-545-155).

BrdU injections

BrdU (Sigma) was injected intraperitoneally 1 time at 50 mg/g body weight, 2 days after electroporation. Mice were sacrificed 2 h after BrdU injection and stained with a rat anti-BrdU antibody (Bio-Rad). BrdU-positive cells among EGFP cells were then counted in the SVZ at 2 dpe using ImageJ software.

Immunohistochemistry and image analysis

For histological analysis, pups were deeply xylazine/ketamine anaesthetized. Perfusion was performed intracardiacally with a solution of 4%

Development (2017) 144, 3968-3977 doi:10.1242/dev.151381

paraformaldehyde in PBS. The brain was dissected out and incubated overnight in the same fixative at 4°C. Sections were cut at 50 µm using a microtome (Microm). Floating sections were first incubated overnight at 4°C with the following primary antibodies: rabbit anti-EGFP (1:500; Life Technologies), mouse anti-NeuN IgG1 (1:100; Merck Millipore, MAB377), rabbit anti-GFAP (1:2000, DAKO, Z0334), mouse anti-S100B (1:1000, Sigma), mouse anti-CRE recombinase (1:4000, Millipore, MAB3120), rat IgG2a anti-BrdU (1:1000, Bio-Rad, OBT0030) before incubation 2 h at room temperature with the corresponding fluorescent labelled secondary antibody. Before mounting, cell nuclei were stained with Hoechst 33258. Optical images were taken either using a fluorescence microscope (Axioplan2, ApoTome system, Zeiss) or a laser confocal scanning microscope (LSM510 or LSM780, Zeiss).

Cytoplasmic fluorescence intensity was measured using ImageJ software on 12-bit *z*-stack images. Each cell was circled, and mean pixel intensity was extracted and normalized to an arbitrary unit (a.u.) corresponding to 4095 bit depth.

qRT-PCR

Mice were killed by decapitation and brains were dissected out. SVZ was micro-dissected from 300 µm vibratome brain sections. RNA was then extracted using the miRNAeasy kit (Qiagen) and cDNA were prepared using super-script III reverse transcriptase (Invitrogen). Quantitative PCR was performed on a Bio-Rad CFX system using SYBR GreenER qPCR SuperMix (Invitrogen). β-Actin was used as a reference gene. The oligonucleotides used for amplification were: β-actin FORseq, CTAAGGCCAACCGTGAAAAG; β-actin REVseq, ACCAGAGGCATACAGGGACA; EGFP FORseq, AGAACGGCATCAAGGTGAAC; EGFP REVseq, GAACTCCAGCAGGACCATGT.

Spine quantification

Images were taken using a laser confocal scanning microscope (LSM780, Zeiss) with a 63× objective. Lateral and *z*-axis resolutions were 100 nm and 380 nm, respectively. Spine density and spine length quantifications were performed on *z*-stack projections using the NeuronJ (Meijering et al., 2004) plug-in of ImageJ software. All dendritic protrusions showing a clearly visible head were quantified as dendritic spines. Imaging and quantifications were all performed blindly to experimental groups.

Statistical analyses

Statistical analyses were performed using R software and R Commander package (https://CRAN.R-project.org/package=Rcmdr). Data are presented as mean±s.e.m. except for Fig. 1J where data are presented as mean±s.d. Non-parametrical Wilcoxon rank sum test was used to assess mean differences between two groups and Kolgomorov–Smirnov test was used to assess differences between distributions (Fig. 6G,J). Differences were considered statistically significant when $P<0.05$ (ns, $P>0.05$; *$P\leq0.05$; **$P\leq0.01$; ***$P\leq0.001$). Levene's test was used to assess equality of variances (Fig. 1J) and variances were considered statistically different if $P<0.05$.

Acknowledgements

Imaging was performed using the PiCSL-FBI core facility (IBDM, AMU-Marseille, France) supported by the Agence Nationale de la Recherche through the 'Investments for the Future' program (France-BioImaging, ANR-10-INBS-04). We acknowledge the IBDM animal facilities. We thank Jean-Claude Platel for fruitful discussions and critical reading of the manuscript.

Competing interests

A.B. and S.W. are employees of Miltenyi Biotec. All other authors declare no competing interests.

Author contributions

Conceptualization: A.B., H.C., C. Beclin; Methodology: S.B., A.d.C., C. Boutin, S.W., A.B., C. Beclin; Formal analysis: S.B., C. Boutin, H.C., C. Beclin; Investigation: S.B., A.d.C., C. Boutin, N.C.; Resources: S.W., A.B.; Writing - original draft: S.B., H.C., C. Beclin; Writing - review & editing: A.d.C., C. Boutin, N.C., A.B.; Supervision: H.C., C. Beclin; Project administration: H.C.; Funding acquisition: H.C.

Funding

H.C. received funding from Agence Nationale de la Recherche (ANR; AtmiR Blanc SVSE 4 201), Fédération pour la Recherche sur le Cervau (FRC), Association France Parkinson and the Fondation de France (FDF; SUBV 2012 00034625). S.B. received funding from Fondation pour la Recherche Médicale (FRM; FDT20160435597). H.C. and A.B. were funded by the European Commission FP7-PEOPLE-2011-IAPP - Marie Curie Action: 'Industry-Academia Partnerships and Pathways' DopaNew.

Supplementary information

Supplementary information available online at
http://dev.biologists.org/lookup/doi/10.1242/dev.151381.supplemental

References

Barnabé-Heider, F., Meletis, K., Eriksson, M., Bergmann, O., Sabelström, H., Harvey, M. A., Mikkers, H. and Frisén, J. (2008). Genetic manipulation of adult mouse neurogenic niches by in vivo electroporation. *Nat. Methods* **5**, 189-196.

Bernstein, E., Kim, S. Y., Carmell, M. A., Murchison, E. P., Alcorn, H., Li, M. Z., Mills, A. A., Elledge, S. J., Anderson, K. V. and Hannon, G. J. (2003). Dicer is essential for mouse development. *Nat. Genet.* **35**, 215-217.

Bertrand, V., Hudson, C., Caillol, D., Popovici, C. and Lemaire, P. (2003). Neural tissue in ascidian embryos is induced by FGF9/16/20, acting via a combination of maternal GATA and Ets transcription factors. *Cell* **115**, 615-627.

Bicker, S., Lackinger, M., Weiß, K. and Schratt, G. (2014). MicroRNA-132, -134, and -138: a microRNA troika rules in neuronal dendrites. *Cell. Mol. Life Sci.* **71**, 3987-4005.

Boutin, C., Diestel, S., Desoeuvre, A., Tiveron, M.-C. and Cremer, H. (2008). Efficient in vivo electroporation of the postnatal rodent forebrain. *PLoS ONE* **3**, e1883.

Boutin, C., Hardt, O., de Chevigny, A., Coré, N., Goebbels, S., Seidenfaden, R., Bosio, A. and Cremer, H. (2010). NeuroD1 induces terminal neuronal differentiation in olfactory neurogenesis. *Proc. Natl. Acad. Sci. USA* **107**, 1201-1206.

Boutin, C., Labedan, P., Dimidschstein, J., Richard, F., Cremer, H., André, P., Yang, Y., Montcouquiol, M., Goffinet, A. M. and Tissir, F. (2014). A dual role for planar cell polarity genes in ciliated cells. *Proc. Natl. Acad. Sci. USA* **111**, E3129-E3138.

Cohen, J. E., Lee, P. R., Chen, S., Li, W. and Fields, R. D. (2011). MicroRNA regulation of homeostatic synaptic plasticity. *Proc. Natl. Acad. Sci. USA* **108**, 11650-11655.

Corish, P. and Tyler-Smith, C. (1999). Attenuation of green fluorescent protein half-life in mammalian cells. *Protein Eng.* **12**, 1035-1040.

de Chevigny, A., Coré, N., Follert, P., Gaudin, M., Barbry, P., Béclin, C. and Cremer, H. (2012). miR-7a regulation of Pax6 controls spatial origin of forebrain dopaminergic neurons. *Nat. Neurosci.* **15**, 1120-1126.

De la Rossa, A. and Jabaudon, D. (2014). In vivo rapid gene delivery into postmitotic neocortical neurons using iontoporation. *Nat. Protoc.* **10**, 25-32.

De Vry, J., Martínez-Martínez, P., Losen, M., Temel, Y., Steckler, T., Steinbusch, H. W. M., De Baets, M. H. and Prickaerts, J. (2010). In vivo electroporation of the central nervous system: a non-viral approach for targeted gene delivery. *Prog. Neurobiol.* **92**, 227-244.

Faedo, A., Laporta, A., Segnali, A., Galimberti, M., Besusso, D., Cesana, E., Belloli, S., Moresco, R. M., Tropiano, M., Fucà, E. et al. (2016). Differentiation of human telencephalic progenitor cells into MSNs by inducible expression of Gsx2 and Ebf1. *Proc. Natl. Acad. Sci. USA* **114**, E1234-E1242.

Fernández, M. E., Croce, S., Boutin, C., Cremer, H. and Raineteau, O. (2011). Targeted electroporation of defined lateral ventricular walls: a novel and rapid method to study fate specification during postnatal forebrain neurogenesis. *Neural Dev.* **6**, 13.

Gu, Q.-H., Yu, D., Hu, Z., Liu, X., Yang, Y., Luo, Y., Zhu, J. and Li, Z. (2015). miR-26a and miR-384-5p are required for LTP maintenance and spine enlargement. *Nat. Commun.* **6**, 6789.

Harfe, B. D., McManus, M. T., Mansfield, J. H., Hornstein, E. and Tabin, C. J. (2005). The RNaseIII enzyme Dicer is required for morphogenesis but not patterning of the vertebrate limb. *Proc. Natl. Acad. Sci. USA* **102**, 10898-10903.

Kotterman, M. A. and Schaffer, D. V. (2014). Engineering adeno-associated viruses for clinical gene therapy. *Nat. Rev. Genet.* **15**, 445-451.

Lim, M.-S., Chang, M.-Y., Kim, S.-M., Yi, S.-H., Suh-Kim, H., Jung, S. J., Kim, M. J., Kim, J. H., Lee, Y.-S., Lee, S. Y. et al. (2015). Generation of dopamine neurons from rodent fibroblasts through the expandable neural precursor cell stage. *J. Biol. Chem.* **290**, 17401-17414.

Lowenstein, P., Mandel, R., Xiong, W., Kroeger, K. and Castro, M. (2007). Immune responses to adenovirus and adeno-associated vectors used for gene therapy of brain diseases: the role of immunological synapses in understanding the cell biology of neuroimmune interactions. *Curr. Gene Ther.* **7**, 347-360.

Luni, C., Giulitti, S., Serena, E., Ferrari, L., Zambon, A., Gagliano, O., Giobbe, G. G., Michielin, F., Knöbel, S., Bosio, A. et al. (2016). High-efficiency cellular reprogramming with microfluidics. *Nat. Methods* **13**, 446-452.

Madisen, L., Zwingman, T. A., Sunkin, S. M., Oh, S. W., Hatim, A., Gu, H., Ng, L. L., Palmiter, R. D., Hawrylycz, M. J., Jones, A. R. et al. (2010). A robust and high-throughput Cre Reporting and characterization system for the whole mouse brain. *Nat. Neurosci.* **13**, 133-140.

Mall, M., Kareta, M. S., Chanda, S., Ahlenius, H., Perotti, N., Zhou, B., Grieder, S. D., Ge, X., Drake, S., Euong Ang, C. et al. (2017). Myt1l safeguards neuronal identity by actively repressing many non-neuronal fates. *Nature* **544**, 245-249.

Meijering, E., Jacob, M., Sarria, J.-C. F., Steiner, P., Hirling, H. and Unser, M. (2004). Design and validation of a tool for neurite tracing and analysis in fluorescence microscopy images. *Cytometry A* **58A**, 167-176.

Merkle, F. T., Mirzadeh, Z. and Alvarez-Buylla, A. (2007). Mosaic organization of neural stem cells in the adult brain. *Science* **317**, 381-384.

Mimoto, M. S. and Christian, J. L. (2011). Manipulation of gene function in Xenopus laevis. *Methods Mol. Biol.* **770**, 55-75.

Mirzadeh, Z., Merkle, F. T., Soriano-Navarro, M., García-Verdugo, J. M. and Alvarez-Buylla, A. (2008). Neural stem cells confer unique pinwheel architecture to the ventricular surface in neurogenic regions of the adult brain. *Cell Stem Cell* **3**, 265-278.

Molotkov, D. A., Yukin, A. Y., Afzalov, R. A. and Khiroug, L. S. (2010). Gene delivery to postnatal rat brain by non-ventricular plasmid injection and electroporation. *J. Vis. Exp.* **43**, e2244.

Morin, X., Jaouen, F. and Durbec, P. (2007). Control of planar divisions by the G-protein regulator LGN maintains progenitors in the chick neuroepithelium. *Nat. Neurosci.* **10**, 1440-1448.

Ohmura, N., Kawasaki, K., Satoh, T. and Hata, Y. (2015). In vivo electroporation to physiologically identified deep brain regions in postnatal mammals. *Brain Struct. Funct.* **220**, 1307-1316.

Pagès, S., Cane, M., Randall, J., Capello, L. and Holtmaat, A. (2015). Single cell electroporation for longitudinal imaging of synaptic structure and function in the adult mouse neocortex in vivo. *Front. Neuroanat.* **9**, 36.

Papale, A., Cerovic, M. and Brambilla, R. (2009). Viral vector approaches to modify gene expression in the brain. *J. Neurosci. Methods* **185**, 1-14.

Pathania, M., Torres-Reveron, J., Yan, L., Kimura, T., Lin, T. V., Gordon, V., Teng, Z.-Q., Zhao, X., Fulga, T. A., Van Vactor, D. et al. (2012). miR-132 enhances dendritic morphogenesis, spine density, synaptic integration, and survival of newborn olfactory bulb neurons. *PLoS ONE* **7**, e38174.

Porrero, C., Rodríguez-Moreno, J., Quetglas, J. I., Smerdou, C., Furuta, T. and Clascá, F. (2016). A simple and efficient in vivo non-viral RNA transfection method for labeling the whole axonal tree of individual adult long-range projection neurons. *Front. Neuroanat.* **10**, 27.

Ribeiro, S., Mairhofer, J., Madeira, C., Diogo, M. M., Lobato da Silva, C., Monteiro, G., Grabherr, R. and Cabral, J. M. (2012). Plasmid DNA size does affect nonviral gene delivery efficiency in stem cells. *Cell. Reprogram.* **14**, 130-137.

Sack, B. K. and Herzog, R. W. (2009). Evading the immune response upon in vivo gene therapy with viral vectors. *Curr. Opin. Mol. Ther.* **11**, 493-503.

Saito, T. and Nakatsuji, N. (2001). Efficient gene transfer into the embryonic mouse brain using in vivo electroporation. *Dev. Biol.* **240**, 237-246.

Siegel, G., Saba, R. and Schratt, G. (2011). MicroRNAs in neurons: Manifold regulatory roles at the synapse. *Curr. Opin. Genet. Dev.* **21**, 491-497.

Siegert, S., Seo, J., Kwon, E. J., Rudenko, A., Cho, S., Wang, W., Flood, Z., Martorell, A. J., Ericsson, M., Mungenast, A. E. et al. (2015). The schizophrenia risk gene product miR-137 alters presynaptic plasticity. *Nat. Neurosci.* **18**, 1008-1016.

Weiss, K., Antoniou, A. and Schratt, G. (2015). Non-coding mechanisms of local mRNA translation in neuronal dendrites. *Eur. J. Cell Biol.* **94**, 363-367.